Hindawi
Shock and Vibration
Volume 2023, Article ID 6050633, 17 pages
https://doi.org/10.1155/2023/6050633

Research Article

Design and Optimization of a New Vibration Damping System for the Driving Characteristics of the Selected Case of Replacing Pneumatic Wheels with Nonpneumatic Wheels

Renkai Ding,[1,2] **Ping Wang**,[1] **Ruochen Wang**,[3] **and Dong Sun**[3]

[1]*State Key Laboratory of Automotive Simulation and Control, Jilin University, Changchun, Jilin 130015, China*
[2]*Automotive Engineering Research Institute, Jiangsu University, Zhenjiang 212013, China*
[3]*School of Automotive and Traffic Engineering, Jiangsu University, Zhenjiang 212013, China*

Correspondence should be addressed to Renkai Ding; drk@ujs.edu.cn

Received 9 August 2023; Revised 1 December 2023; Accepted 7 December 2023; Published 22 December 2023

Academic Editor: Peter Múčka

To cope with the deterioration of vehicle dynamic performance induced by the increased mass and vertical stiffness of selected nonpneumatic wheels (NPWs), this study proposed a new vibration damping system (NVDS) based on the dynamic vibration absorber (DVA). First, a quarter-vehicle model containing the effective vertical stiffness of the NPW is established. Then, the effect of increased wheel mass and stiffness on vehicle dynamic performance is investigated from various aspects. To improve the handling performance of the vehicle with NPWs, a DVA-based NVDS is proposed. The sensitivities of handling performance and ride comfort to parameter changes are investigated to determine the selection range of parameters. The multiobjective genetic algorithm (GA) is employed to determine the optimal parameters of NVDS. The results obtained under different road excitations indicate that the proposed NVDS can significantly enhance the handling performance and ride comfort of the vehicle.

1. Introduction

The wheel is a critical component of the vehicle system, which is utilized to support the vehicle load, ensure good contact with the road, and attenuate the road impact [1]. Owing to its good adaptability to road roughness and ability to absorb shock, the pneumatic wheel is widely used in passenger and commercial vehicles [2]. Although the pneumatic wheel has been proven to have superior performance, its deficiencies are also obvious, such as the complex manufacturing process, expensive production costs, difficult recycling, and the loss of vehicle control in the event of bursting [3]. In other words, the wheel performance not only influences the dynamic performance but also relates to the vehicle's safety.

To overcome the shortcomings of traditional pneumatic wheels, various improved technologies have been put forward by manufacturers and research institutions, such as the run-flat technology [4], sealant technology [5], and internal support technology [6]. However, the above technology can only maintain the basic driving performance of the vehicle after a leak or puncture, which cannot fundamentally prevent punctures. To ensure the normal operation of the vehicle, it is essential to prevent punctures [7]. The emergence of NPW broke through the bottleneck of the current technology. Due to the special structure design and material application, it can not only realize the basic functions of a pneumatic wheel but also have the characteristics of puncture resistance and damage prevention, which fundamentally avoid the risk of wheel puncture. Thus, research on NPWs has been actively conducted recently. In terms of structure, various types of NPWs are developed, including Tweel NPW [8], honeycomb wheel [9–11], spoke NPW [12, 13], and nonpneumatic mechanical elastic wheel (ME-wheels) [14–16]. In terms of stiffness characteristics, Zhang et al. [17] designed a flexible spoke NPW based on the bionic concept, established its radial stiffness coupling model through numerical and theoretical derivation,

and validated the accuracy of the model through test. Gasmi et al. [18] simplified the tread of the NPW as a bending beam and the spokes as springs and constructed a quasi-static, two-dimensional analysis model. Additionally, various studies regarding wheel ground contact behaviour [19–21], rolling resistance [22, 23], and fatigue life [24, 25] are also conducted by scholars.

It can be seen that remarkable progress has been made in the research on the structure and basic characteristics of NPWs. However, how to realize the effective and comprehensive application remains to be explored. The radial stiffness of NPWs is significantly higher than that of pneumatic wheels and shows obvious nonlinearity [26, 27]. Therefore, its application to existing vehicles will inevitably lead to the deterioration of a series of dynamic performance, such as the ride comfort and handling performance. To address this problem, Dhrangdhariya et al. [28] studied the influence of different nonlinear materials and spoke structures on wheel stiffness and proposed the best combination of them that can enhance the ride comfort. Zhou et al. [29] developed an asymmetric spoke structure and optimized its structural parameters, which effectively improved the vibration damping performance of spoke NPWs. It should be noted that the optimization of structural parameters and materials has a limited effect on the improvement of ride comfort due to the contradiction between support and damping properties. On the other hand, the suspension and wheels work together to attenuate the road impact during driving. Thus, suspension matching and control strategy design may be another way to enhance the dynamic performance of the vehicle with NPWs, which is not involved in current research. Although Wang et al. [30] improved the dynamic performance of vehicles with ME-wheels through an adaptive feedback control strategy, the specific effects of ME-wheels on dynamic performance were not clarified. The main purpose of this work is to explore effective ways to improve the vehicle's dynamic performance based on a clear understanding of the impact of the selected NPW.

The main contributions include the analysis of the effect of NPW mass and vertical stiffness on vehicle dynamic performance from different aspects, the design of an NVDS consisting of a passive suspension and a DVA, and the optimization of system parameters. It is shown that the proposed NVDS can reduce vehicle body and wheel vibration on different roads. The remainders are organized as follows: Section 2 describes the modelling of a quarter-vehicle model, and Section 3 analyses the effects of NPW mass and vertical stiffness on vehicle dynamic performance. Section 4 presents the design and optimization of the NVDS based on DVA using multiobjective GA. Section 5 gives the results and discussion. The general conclusions are drawn in Section 6.

2. Vehicle System Modelling

2.1. Identification of Effective Vertical Stiffness of NPW. This study focuses on the improvement of the vertical dynamic performance of the vehicle which directly related to the wheel's vertical stiffness. To obtain the vertical stiffness of the NPWs, static load-deflection tests were performed. A commercially available 155/60R13 NPW designed for the automobiles, as shown in Figure 1(a), was used in this study. The overall diameter of the wheel was 508 mm, and it adopted a staggered O-type rubber structure. The multifunctional experimental bench used for the static load-deflection experiment is shown in Figure 1(b). It was mainly constructed of an inertial frame fixed to the ground, a moving frame restricted to move in a vertical direction, a force transducer placed between the moving frame and the inertial frame, and an oscilloscope. The force transducer is used to measure the vertical force of the wheel during the loading, and its value can be directly read by the oscilloscope. In the experiment, the vertical deflection of the wheel increased from 0 mm to 17 mm with a step of 0.5 mm, and the load was recorded. The same experiment was performed for a reference pneumatic wheel with the same size (155/60R13). The air pressure in the pneumatic wheel is 240 kPa, a commonly used air pressure in passenger vehicles.

The relationship between the load and vertical deflection for both wheels is given in Figure 1(c). It is clear that the vertical stiffness of the NPW is greater than that of the pneumatic wheel and exhibits a significant nonlinearity. The vertical stiffness of the pneumatic wheel is linear, which is 128000 N/m according to the experimental data. The effective stiffness of the NPW calculated in the vicinity of the operating static load (~362.9 kg) is adopted for the subsequent analysis, which is 332900 N/m. The masses of pneumatic wheel and nonpneumatic wheel were also measured, which were 17.4 kg and 23.3 kg, respectively. Considering that the measurement process is very simple and common, it is not described in detail here.

2.2. Quarter-Vehicle Model. To study the effects of NPW on vehicle dynamic performance, a quarter-vehicle model that can reflect the vertical vibration characteristics of the vehicle is established, as shown in Figure 2. The dynamics equation can be derived based on Newton's second law as follows:

$$m_2\ddot{z}_2 + c_1(\dot{z}_2 - \dot{z}_1) + k_2(z_2 - z_1) = 0, \quad (1a)$$

$$m_1\ddot{z}_1 - c_1(\dot{z}_2 - \dot{z}_1) - k_2(z_2 - z_1) + k_1(z_1 - z_0) = 0, \quad (1b)$$

where m_1 is the unsprung mass (herein, $m_1 = 36.6$ kg for the vehicle with pneumatic wheels and $m_1 = 45.4$ kg for the vehicle with NPWs); m_2 is the sprung mass (herein, $m_2 = 317.5$ kg); c_1 is the suspension damping (herein, $c_1 = 1500$ N·s/m); k_2 is the suspension stiffness (herein, $k_2 = 20000$ N/m); k_1 is the wheel/wheel stiffness (herein, $k_1 = 128000$ N/m for pneumatic wheel and $k_1 = 332900$ N/m for NPW); z_0 is the road excitation; and z_1 and z_2 are the motions of the unsprung and sprung masses, respectively.

Through Laplace transform of equations (1a) and (1b), we can obtain the following equation:

$$\begin{cases} z_2\left(m_2s^2 + c_1s + k_s\right) - z_1(c_1s + k_2) = 0, \\ -z_2(c_1s + k_2) + z_1\left(m_1s^2 + c_1s + k_2 + k_1\right) - z_0k_1 = 0. \end{cases} \quad (2)$$

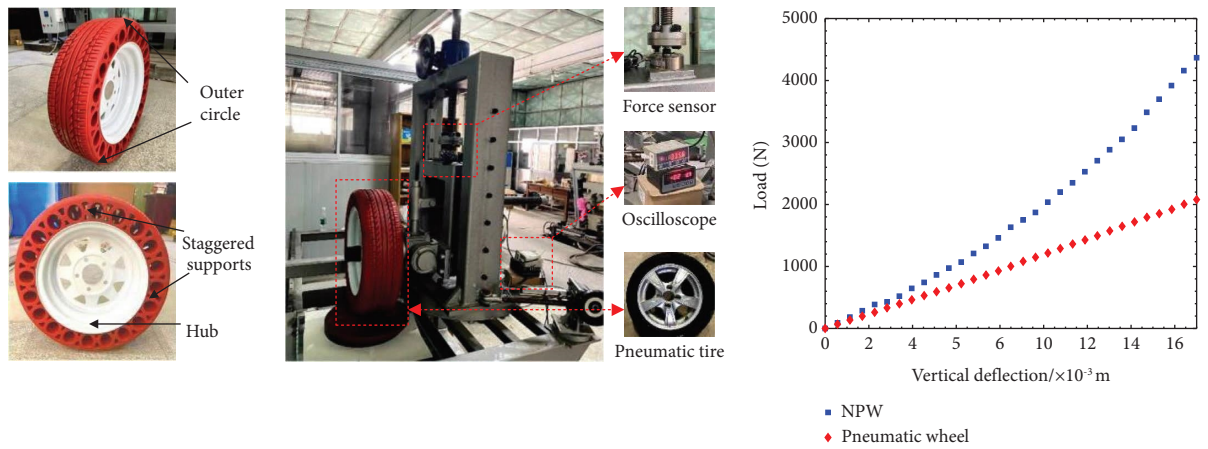

Figure 1: Static load-deflection experiment: (a) structure of NPW; (b) experimental bench arrangement; (c) experimental results.

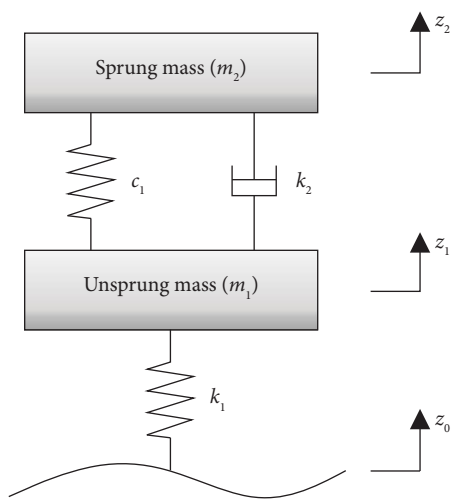

Figure 2: Quarter-vehicle model.

Then, the transfer function between z_2 and z_1, z_1 and z_0, and z_2 and z_0 can be derived as follows:

$$\frac{z_2}{z_1} = \frac{A_1}{A_2}, \tag{3}$$

$$\frac{z_2}{z_0} = \frac{A_1 k_1}{A_2 A_3 - A_1^2}, \tag{4}$$

$$\frac{z_1}{z_0} = \frac{A_2 k_1}{A_2 A_3 - A_1^2}, \tag{5}$$

where $A_1 = m_2 s^2 + c_1 s + k_2$, $A_2 = c_1 s + k_2$, and $A_3 = m_1 s^2 + c_1 s + k_2 + k_1$.

2.3. Road Excitation Model. As shown in Figure 2, the road excitation is the only disturbance source in the quarter-vehicle model. To analyse the dynamic performance of vehicles under different road excitations, the random road with statistical characteristics and the bump road with discrete characteristics are used as the input. Furthermore, a sinusoidal road excitation was also adopted to investigate the vibration response of the vehicle with NPWs under specific frequency excitation, which is a relatively simple model and is not elaborated here.

2.3.1. Random Road Excitation. Since the random road can be regarded as a white noise signal with a finite bandwidth, the road excitation signal can be generated by a white noise passed through a filter [31]. The model of random road excitation in the time domain constructed by the filtered white noise method can be expressed as follows:

$$\dot{z}_0(t) = -2\pi f_0 z_0(t) + 2\pi n_0 \sqrt{G_q(n_0) v} \cdot w(t), \tag{6}$$

where f_0 is the lower cut-off frequency, generally taken as 0.011; v is the vehicle speed; n_0 is the reference spatial frequency and $n_0 = 0.1$; $G_q(n_0)$ is the spatial spectral density corresponding to the reference spatial frequency, also known as the road unevenness coefficient, and the corresponding relationship between it and the road classes is defined as ISO 8608 [32]; and $w(t)$ is the white noise signal with zero mean value.

In this paper, the class B and C roads are taken as system input for dynamics simulation analysis, and the geometric mean of $G_q(n_0)$ is adopted to generate the random road excitation. Specifically, $G_q(n_0) = 64 \times 10^{-6}\,\mathrm{m}^3$ is selected for class B road, as well as $G_q(n_0) = 256 \times 10^{-6}\,\mathrm{m}^3$ is selected for class C road. Assuming that the vehicle travels on class B and C roads at a speed of 60 km/h, the road excitations generated using equation (6) are shown in Figure 3(a). It is obvious that the amplitude of class C road is greater than that of class B road, which will lead to more severe vibration of the vehicle.

2.3.2. Bump Road Excitation. To study the dynamic response characteristics of the vehicle on a discrete road, a model of bump road excitation is established as follows [33] (Jiang et al. 2021):

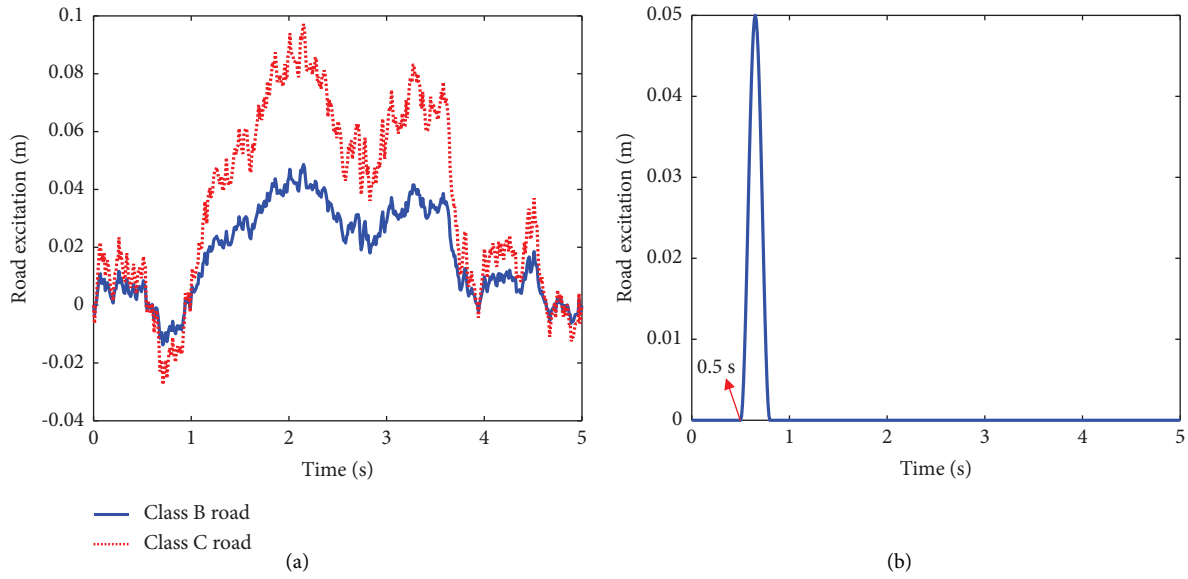

Figure 3: Road excitation: (a) random road and (b) bump road.

$$z_0 = \begin{cases} \frac{h}{2}\left(1 - \cos\left(2\pi \cdot \frac{v}{l} \cdot t\right)\right), & t_1 < t < \frac{l}{v}, \\ 0, \text{other}, \end{cases} \tag{7}$$

where h and l are the height and length of the bump, respectively; t_1 is the starting time when the vehicle passes the bump; here, $h = 0.05$ m, $l = 5$ m, and $t_1 = 0.5$ s. Considering that the speed of vehicles passing through bumpy roads is usually not high, the speed is assumed to be 36 km/h here. Figure 3(b) depicts the generated bump road excitation.

3. Effects of NPWs on the Dynamic Performance of the Vehicle

The analysis shows that the selected NPW has greater mass and vertical stiffness compared to the reference pneumatic wheel, which will inevitably cause the variation in the vehicle vibration response and may even deteriorate the vehicle's dynamic performance. Therefore, clarifying the effect of NPW on vehicle vertical vibration is essential to improving the dynamic performance and promoting the application of NPWs. In the following, the effects of NPW mass and stiffness on vehicle vibration response are comprehensively analysed from the perspective of frequency domain, time domain, and power flow.

3.1. Analysis of Frequency-Domain Response. For the quarter-vehicle model, the vehicle body acceleration (VBA), suspension rattle space (SWS), and relative dynamic wheel load (DWL) are usually used to evaluate its ride comfort and handling performance. These three indicators can well reflect the vertical dynamic performance of the vehicle at different frequencies. To acquire the effects of the NPW on the dynamic performance of the vehicle in the frequency domain, the amplitude-frequency characteristics were analysed. For the linear suspension system model, the frequency-domain transfer function is usually used to analyse the amplitude-frequency response characteristics [34, 35]. The relevant formulas for calculating the frequency-domain transfer function of a linear suspension system are provided below.

The amplitude-frequency characteristics of the VBA $\ddot{z}_2$ to the road excitation speed $\dot{z}_0$ can be expressed as follows:

$$|H(j\omega)|_{\ddot{z}_2 \sim \dot{z}_0} = \left|\frac{\ddot{z}_2}{\dot{z}_0}\right| = \omega\left|\frac{z_2}{z_0}\right|. \tag{8}$$

Substituting equation (4) into equation (8), we can obtain

$$|H(j\omega)|_{\ddot{z}_2 \sim \dot{z}_0} = \left|\frac{\omega A_1 k_1}{A_2 A_3 - A_1^2}\right|. \tag{9}$$

The amplitude-frequency characteristic of the SRS f_d to the road excitation speed $\dot{z}_0$ can be expressed as follows:

$$|H(j\omega)|_{f_d \sim \dot{z}_0} = \left|\frac{f_d}{\dot{z}_0}\right| = \frac{1}{\omega}\left|\frac{z_2 - z_1}{z_0}\right|. \tag{10}$$

Substituting equations (4) and (5) into equation (10), we can obtain

$$|H(j\omega)|_{f_d \sim \dot{z}_0} = \left|\frac{k_1(A_1 - A_2)}{\omega\left(A_2 A_3 - A_1^2\right)}\right|. \tag{11}$$

The amplitude-frequency characteristic of relative DWL F_d/G to the road excitation speed $\dot{z}_0$ can be expressed as follows:

$$|H(j\omega)|_{F_d \sim \dot{z}_0} = \left|\frac{F_d/G}{\dot{z}_0}\right| = \left|\frac{z_1 - z_0}{z_0}\right| \times \frac{k_1}{\omega(m_1 + m_2)g}, \tag{12}$$

where $F_d = k_1(z_1 - z_0)$ is the DWL and $G = (m_1 + m_2)g$ is the static wheel load.

Substituting equation (5) into equation (12), we can obtain

$$|H(j\omega)|_{F_d \sim \dot{z}_0} = \frac{k_1\left[A_2(k_t - A_3) + A_1^2\right]}{\omega\left(A_2A_3 - A_1^2\right)(m_1 + m_2)g}. \tag{13}$$

According to the above transfer functions of the amplitude-frequency characteristics, the curves of the dynamic responses in the frequency domain can be obtained by MATLAB software. The amplitude-frequency response curves of the VBA, SWS, and relative DWL are shown in Figure 4. It can be observed that the amplitude-frequency characteristics of the vehicle with pneumatic wheels and with NPWs are basically the same within the 2~8 Hz. In case of the vehicle body resonance, the amplitudes of VBA, SWS and relative DWL are slightly lower for the vehicle with NPWs than for the vehicle with pneumatic wheels, which was caused by the increased wheel mass. However, the response amplitude of the vehicle with NPW was significantly larger in the case of wheel resonance due to the increased wheel stiffness. Furthermore, the vehicle with NPWs occurs for wheel resonance at a frequency of 13.5 Hz, which is higher than that of the vehicle with pneumatic wheels. Overall, NPW exacerbates high-frequency vibrations in the vehicle, leading to deterioration of ride comfort and handling performance.

As shown in equation (6), the random road excitation is related to the vehicle speed and road roughness properties. The dynamic response of the vehicle varies for different road excitations. As a result, the effects of vehicle speed and road roughness variation on the frequency-domain response of the vehicle under random road excitation were investigated separately. Assuming that the vehicle runs on a class B road at speeds of 36 km/h, 72 km/h and 108 km/h, the calculated vertical vibration response is as shown in Figure 5. It can be seen that the amplitudes of the power-spectral-density (PSD) curves of three evaluation indicators increase with increasing vehicle speed. In other words, the increase in vehicle speed exacerbates the vertical vibration and deteriorates the ride comfort and handling performance. The overall trend of the PSD curves is similar to that of the corresponding amplitude-frequency characteristic curves.

Similarly, assuming that the vehicle travels at 72 km/h on class A~ C roads, the vibration response can be obtained as shown in Figure 6. It is clear that the amplitudes of the PSD curves for VBA, SRS, and relative DWL increase significantly with increasing road roughness in the full frequency band. According to Figures 5 and 6, it can be seen that the increase in road roughness has a greater effect on the vibration response of the vehicle than the increase in vehicle speed, which will drastically deteriorate the ride comfort and handling performance of the vehicle with NPWs.

3.2. Analysis of Time-Domain Response. The vibration response of the vehicle was also calculated under different road conditions in the time domain to further study the effect of NPWs. The root mean square (RMS) values of the VBA, SRS, and DWL are adopted to evaluate the vehicle's dynamic performance in the time domain. Assuming that the vehicle runs on the class B and C roads at different vehicle speeds, the statistical results of three evaluation indicators can be calculated.

As shown in Figure 7, the higher the vehicle speed, the greater the time-domain responses of the vehicle will be, and hence, the less ride comfort as well as handling performance will be. The RMS values of VBA and DWL of the vehicle with NPWs are significantly larger than those of the vehicle with pneumatic wheels, and the difference between them increases further as the vehicle speed increases. In other words, the ride comfort and handling performance of the vehicle with NPWs deteriorates faster as vehicle speed increases. On the other hand, the RMS values of SRS at different vehicle speeds are almost the same for both vehicles. This means that the SRS is not sensitive to the increase in NPW stiffness and mass. Similarly, it can be seen that an increase in road roughness has a greater impact on the vehicle's dynamic performance. In addition, it can be seen that the deterioration of the DWL is greater than the VBA as the vehicle speed or road roughness increases, which will lead to a great deterioration of the handling performance. In general, the analysis in the time domain is consistent with that in the frequency domain.

3.3. Power Flow Analysis. To clarify the energy conversion and transfer relationship in the quarter vehicle-road coupled system and seek an effective method to improve the vehicle's dynamic performance, a power flow analysis was conducted. As shown in Figure 2, the road excitation is the power source. The input power flow is transferred to the vehicle body through the wheel and suspension. To derive the calculation equation of the power flow, the equation (1b) can be rewritten as follows:

$$m_1\ddot{z}_1 + m_2\ddot{z}_2 + k_1(z_1 - z_0) = 0. \tag{14}$$

Multiplying both sides of equation (1a) by $(\dot{z}_2 - \dot{z}_1)$ and both sides of equation (14) by $(\dot{z}_1 - \dot{z}_0)$, the following equations can be obtained:

$$m_2\ddot{z}_2\dot{z}_2 + c_1(\dot{z}_2 - \dot{z}_1)^2 + k_2(z_2 - z_1)(\dot{z}_2 - \dot{z}_1) = m_2\ddot{z}_2\dot{z}_1, \tag{15a}$$

$$m_1\ddot{z}_1(\dot{z}_1 - \dot{z}_0) + m_2\ddot{z}_2(\dot{z}_1 - \dot{z}_0) + k_1(z_1 - z_0)(\dot{z}_1 - \dot{z}_0) = 0. \tag{15b}$$

Substituting equation (15a) into equation (15b), the energy conservation equation can be obtained as follows:

$$\begin{aligned} m_1\ddot{z}_1\dot{z}_1 + m_2\ddot{z}_2\dot{z}_2 + c_1(\dot{z}_2 - \dot{z}_1)^2 + k_2(z_2 - z_1)(\dot{z}_2 - \dot{z}_1) \\ + k_1(z_1 - z_0)(\dot{z}_1 - \dot{z}_0) = m_1\ddot{z}_1\dot{z}_0 + m_2\ddot{z}_2\dot{z}_0, \end{aligned} \tag{16}$$

where $(m_1\ddot{z}_1\dot{z}_0 + m_2\ddot{z}_2\dot{z}_0)$ is the power flow input to the quarter-vehicle model by road excitation; $m_1\ddot{z}_1\dot{z}_1$ and $m_2\ddot{z}_2\dot{z}_2$ are the change rates of the kinetic energy for the vehicle body and wheel, respectively; $c_1(\dot{z}_2 - \dot{z}_1)^2$ is the energy dissipated by the suspension damper; $k_2(z_2 - z_1)(\dot{z}_2 - \dot{z}_1)$

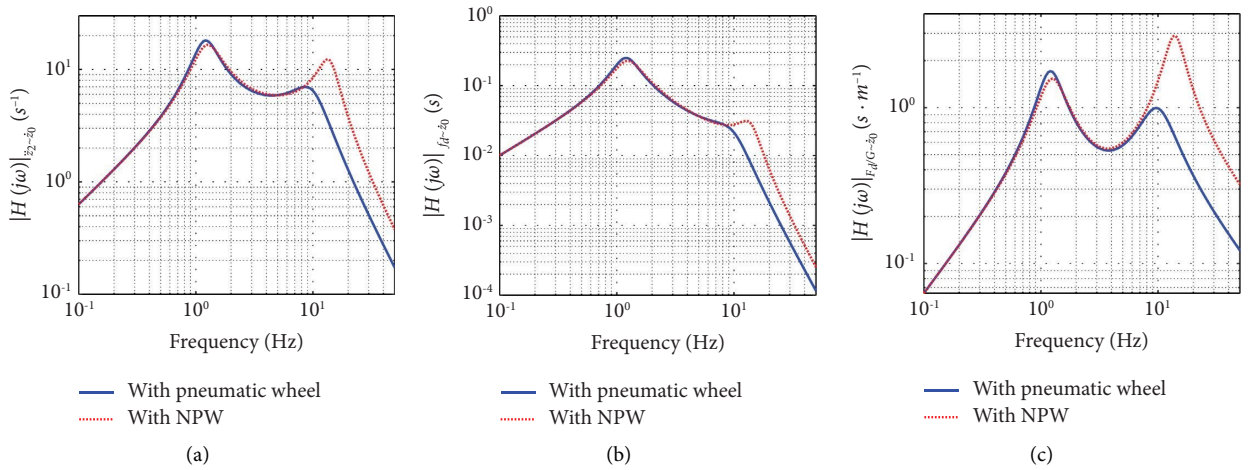

Figure 4: Amplitude-frequency characteristic curves: (a) $\ddot{z}_2 \sim \dot{z}_0$; (b) $f_d \sim \dot{z}_0$; and (c) $F_d/G \sim \dot{z}_0$.

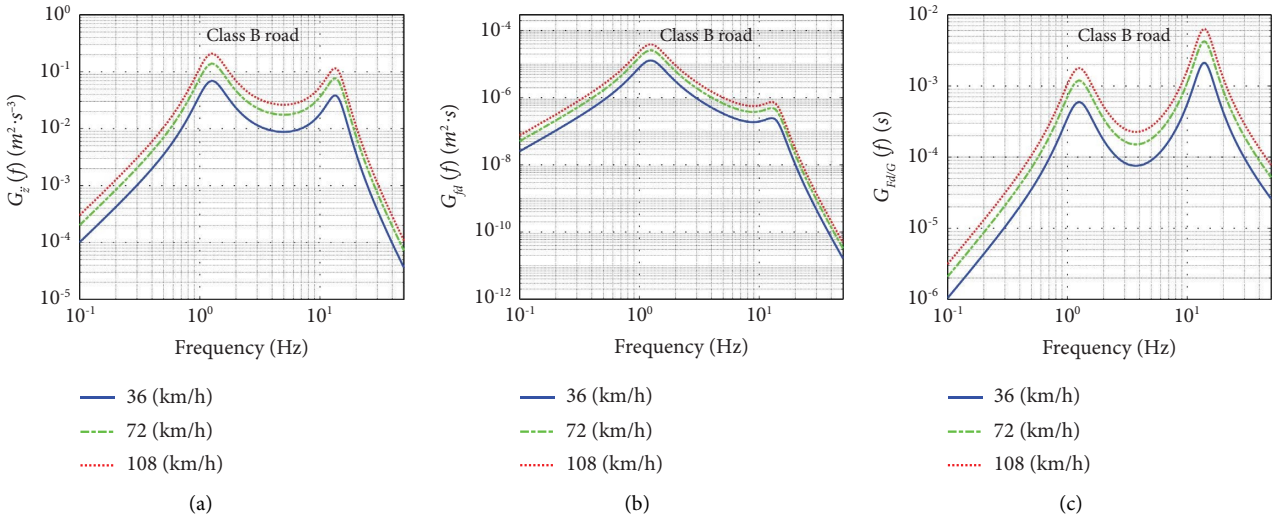

Figure 5: PSD curves of three evaluation indicators on class C road at different speeds: (a) VBA; (b) SRS; and (c) relative DWL.

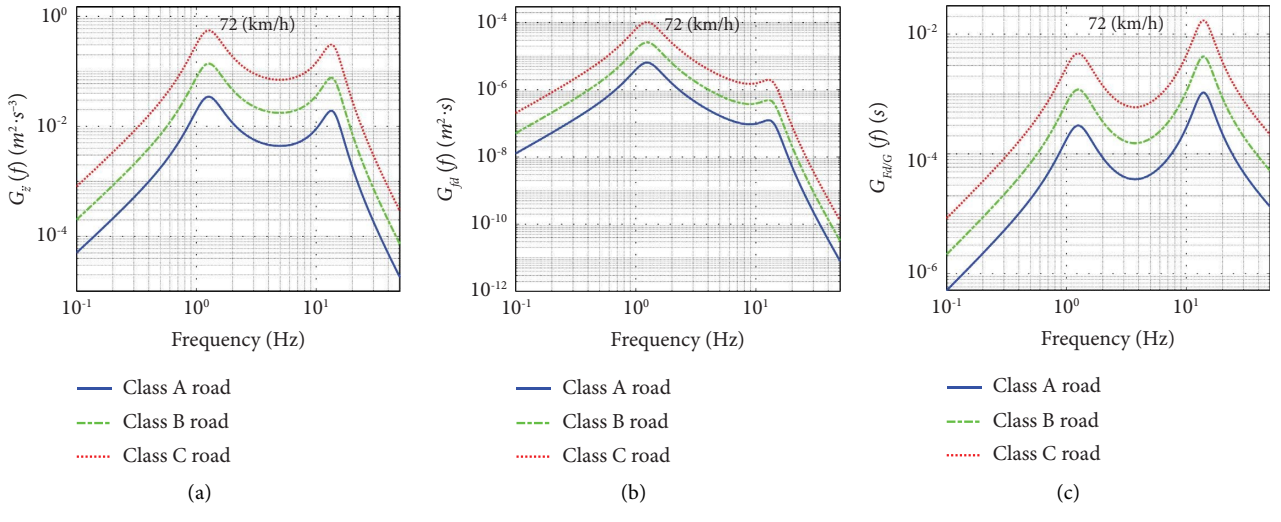

Figure 6: PSD curves of three evaluation indicators at 72 km/h speed on different roads: (a) VBA; (b) SRS; (c) relative DWL.

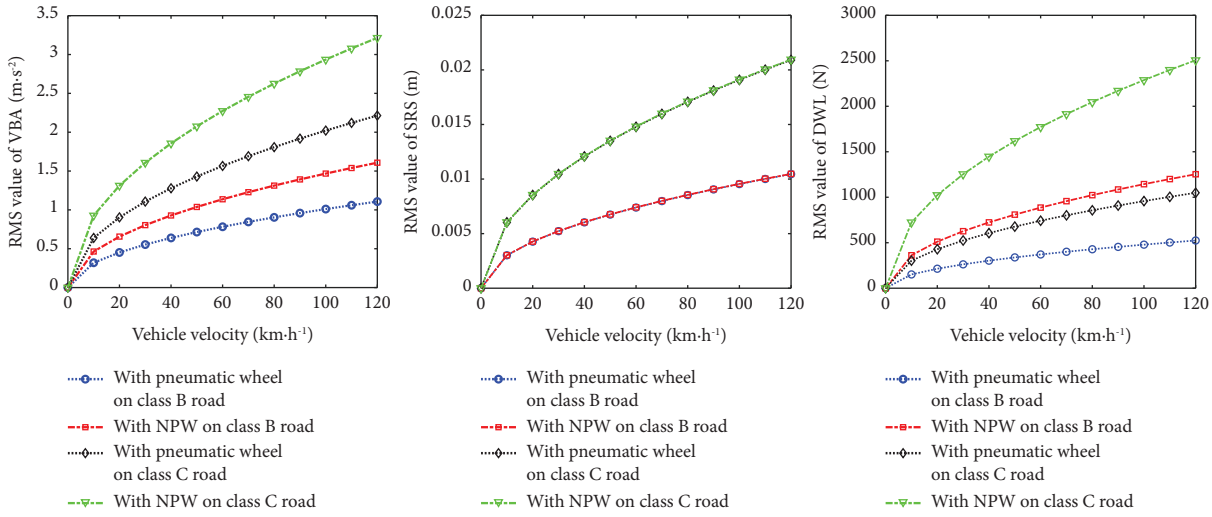

Figure 7: Comparison of the vibration response in the time domain.

and $k_1(z_1 - z_0)(\dot{z}_1 - \dot{z}_0)$ are the change rates of the potential energy for the suspension spring and NPW, respectively.

Since the symbol of power flow only represents the direction, its absolute value is used for analysis. Furthermore, the average power is usually more meaningful for the power flow analysis. The time-averaged input power flow can be defined as follows:

$$\overline{P}_{\text{input}} = \frac{1}{T}\int_0^T \left| m_1 \ddot{z}_1 \dot{z}_0 + m_2 \ddot{z}_2 \dot{z}_0 \right| \mathrm{d}t. \tag{17}$$

Similarly, the time-averaged kinetic energy of vehicle body and wheel is defined as follows:

$$\begin{aligned} \overline{P}_{\text{body}} &= \frac{1}{T}\int_0^T \left| m_2 \ddot{z}_2 \dot{z}_2 \right| \mathrm{d}t, \\ \overline{P}_{\text{tire(kinetic)}} &= \frac{1}{T}\int_0^T \left| m_1 \ddot{z}_1 \dot{z}_1 \right| \mathrm{d}t. \end{aligned} \tag{18}$$

The time-averaged energy dissipated by the suspension damper is defined as follows:

$$\overline{P}_{\text{damper}} = \frac{1}{T}\int_0^T \left| c_1 (\dot{z}_2 - \dot{z}_1)^2 \right| \mathrm{d}t. \tag{19}$$

The time-averaged potential energy of spring and wheel is defined as follows:

$$\begin{aligned} \overline{P}_{\text{spring}} &= \frac{1}{T}\int_0^T \left| k_2 (z_2 - z_1)(\dot{z}_2 - \dot{z}_1) \right| \mathrm{d}t, \\ \overline{P}_{\text{tire(potential)}} &= \frac{1}{T}\int_0^T \left| k_1 (z_1 - z_0)(\dot{z}_1 - \dot{z}_0) \right| \mathrm{d}t. \end{aligned} \tag{20}$$

Based on the above analytical formula, the average power of both vehicles is calculated on class B and C roads at different vehicle speeds, as shown in Figure 8. It can be seen that the average power of each part for both vehicles increases with the vehicle speed. The average power of all parts of the vehicle with NPWs was greater than that of the vehicle with pneumatic wheels, and the difference between them increased with the vehicle speed. In addition, it can be seen that the greatest difference in wheel kinetic energy is between the two vehicles. The above differences in the average energy of the vehicle components are all caused by the wheels, which is the only difference between the two vehicles.

Specifically, as shown in Figure 8(a), the average input power increases significantly with the vehicle speed. The increase of the input power led to an increase in the average power of all parts, including the wheel, spring, and damper. Similarly, it is clear that the increase in road roughness has a greater effect on the average input power compared to the increase in vehicle speed. As shown in Figure 8(c), on both class B and C roads, the average change rate in wheel kinetic energy is significantly greater for the vehicle with NPWs than for the vehicle with pneumatic wheels, i.e., the NPWs lead to further deterioration of vehicle handling performance. As shown in Figure 8(f), the difference in vehicle body kinetic energy is less than that in wheel kinetic energy. The main reason for this is that the suspension damper dissipates more of the vibration energy. As shown in Figure 8(d), the average dissipation energy of the damper in a vehicle with NPWs increases rapidly with increasing vehicle speed and road roughness. The more energy dissipated by the suspension damper, the greater the potential for vibration energy regeneration. This can provide a new idea for the research on vibration energy regeneration, which will not be further discussed here. Similarly, the difference in spring potential energy between both vehicles (shown in Figure 8(e)) is smaller than that in wheel potential energy (shown in Figure 8(b)), also due to the suspension damper. In summary, the increased mass and stiffness of the NPW result in more input energy

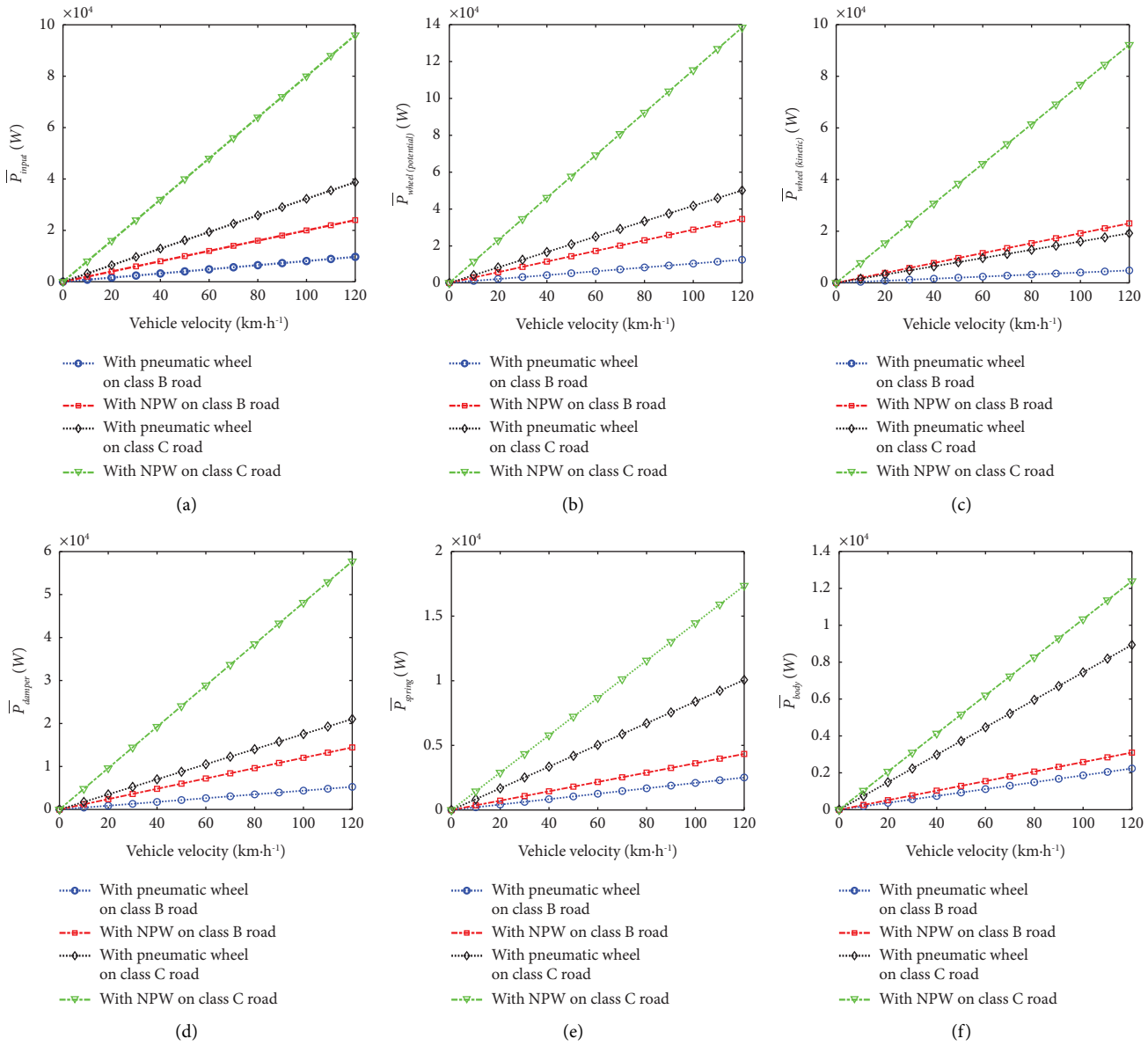

FIGURE 8: Power flow analysis: (a) average input power flow; (b) average potential energy of the wheel; (c) average kinetic energy of the wheel; (d) average energy dissipated by the damper; (e) average potential energy of the spring; (f) average kinetic energy of the vehicle body.

and greater change rates of the kinetic energy of the vehicle body and wheel, which deteriorate the ride comfort and handling performance of the vehicle.

It can be observed from the above analysis that the suspension stiffness and damping have an important effect on the power flow of the quarter vehicle. Therefore, the effect of suspension stiffness and damping on the change rates of the kinetic energy of the vehicle body and wheel was further investigated, as shown in Figure 9. It can be seen that the average change rate of wheel kinetic energy decreases as the suspension damping increases. The greater the suspension damping, the slower the change rate of wheel kinetic energy increases with the vehicle speed. In other words, the tuning of suspension damping can help improve the handling performance of the vehicle. However, the increasing suspension damping may lead to an increase in the change rate of vehicle body kinetic energy (as shown in Figure 9(a)), which deteriorates the ride comfort of the vehicle. As shown in Figures 9(c) and 9(d), the average kinetic energy of the vehicle body and wheel tends to change in opposite directions as the suspension stiffness increases. The average kinetic energy of the vehicle body increases with suspension stiffness, while that of the wheel decreases. In addition, the suspension stiffness has very little effect on wheel kinetic energy. In summary, the suspension stiffness and damping have an important effect on the kinetic energy of the vehicle body and wheel. The reasonable selection of suspension stiffness and damping can help improve the comprehensive performance of the vehicle with NPWs.

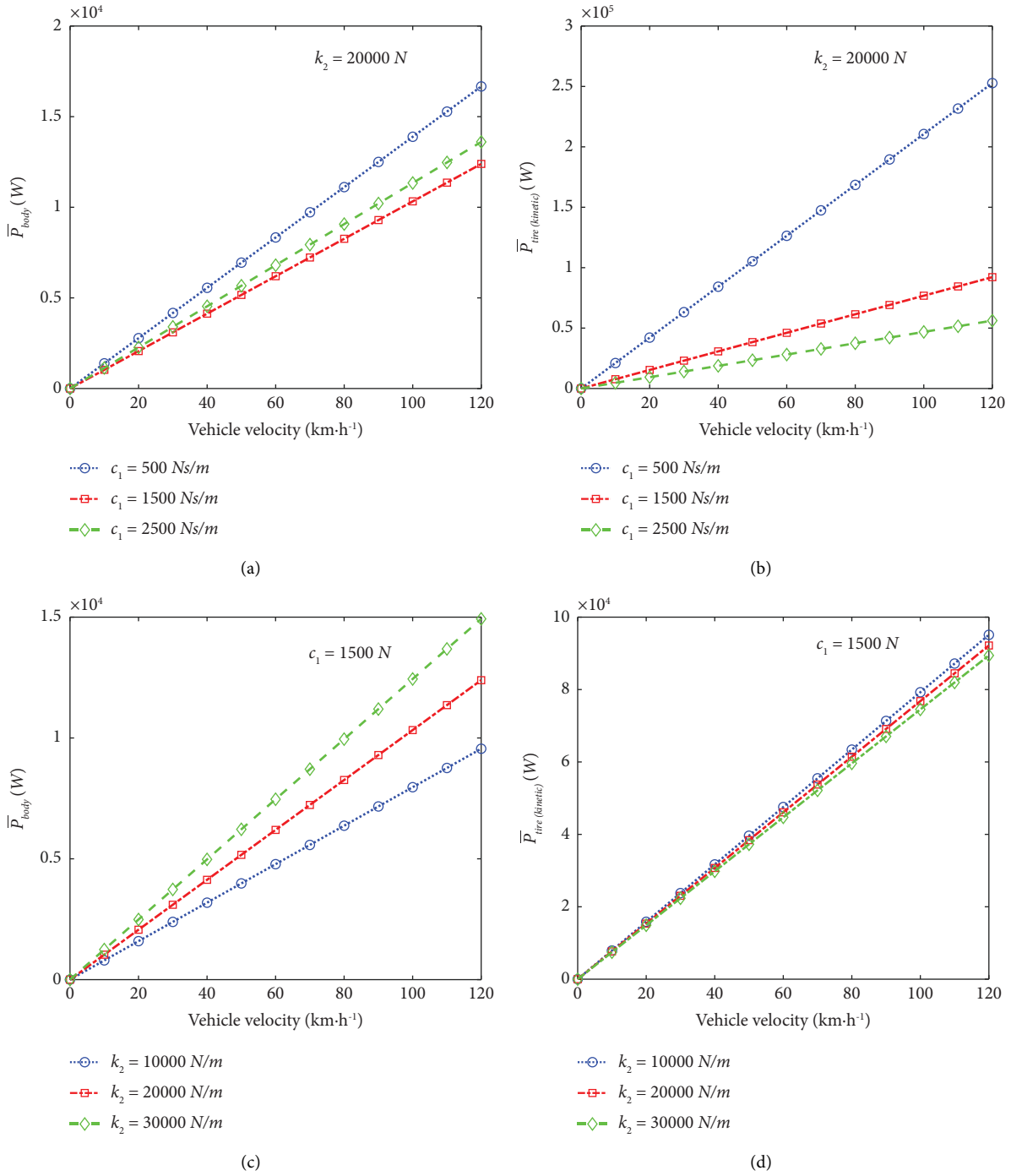

FIGURE 9: Average kinetic energy of vehicle body and wheel at different suspension damping and stiffness: (a) and (c) vehicle body; (b) and (d) wheel.

According to the above analysis from different aspects, the following conclusions can be drawn:

(1) The increased mass and stiffness of NPW will lead to the deterioration of the dynamic performance of the vehicle in the case of wheel resonance, especially the handling performance. Moreover, the increase of the vehicle speed and road roughness will further aggravate the deterioration.

(2) The increased vehicle speed and road roughness led to the faster increase of the average input power of the vehicle with NPWs than the vehicle with pneumatic wheels, resulting in the greater average

kinetic energy of the vehicle body and wheel, which is the fundamental reason for the deterioration of ride comfort and handling stability. Similarly, the increased average energy dissipated by the suspension damper reveals the greater potential for energy regeneration in the vehicle with NPWs.

(3) The suspension stiffness and damping have a significant effect on the average kinetic energy of the vehicle body and wheel. The optimization of suspension stiffness and damping may be a feasible way to improve the dynamic performance of the vehicle with NPWs.

It should be emphasized that the conclusions drawn above only apply to the selected cases in this paper and cannot be generalized to all situations where nonpneumatic wheels are used instead of pneumatic wheels.

4. NVDS Design and Parameter Optimization

4.1. Proposal and Parameter Sensitivity Analysis. Based on the analysis, it is obvious that the first thing to address is the handling performance of vehicles with NPWs, followed by ride comfort. Currently, there are two main approaches used to attenuate vehicle vibration: one is the active approach that realizes the vibration attenuation through the controllable suspensions with advanced control strategies, and the other one is the passive approach that attenuates vibrations by means of properly designed DVA. It should be noted that the active approach requires not only actuator matching and control strategy design but also additional vehicle sensors, which greatly increases production costs. Therefore, a passive approach was adopted in this study, i.e., a DVA-based NVDS was designed. The NVDS consists of a passive suspension and a DVA placed on the unsprung mass, as shown in Figure 10, and its dynamics differential equation can be expressed as follows:

$$\begin{cases} m_3\ddot{z}_3 + c_2(\dot{z}_3 - \dot{z}_1) + k_3(z_3 - z_1) = 0, \\ m_2\ddot{z}_2 + c_1(\dot{z}_2 - \dot{z}_1) + k_2(z_2 - z_1) = 0, \\ m_1\ddot{z}_1 - c_2(\dot{z}_3 - \dot{z}_1) - c_1(\dot{z}_2 - \dot{z}_1) - k_3(z_3 - z_1) - k_2(z_2 - z_1) + k_1(z_1 - z_0) = 0, \end{cases} \tag{21}$$

where m_3, c_2, and k_3 are the mass, damping, and stiffness of the DVA to be determined, respectively.

The DVA is composed of an elastic element, a damping element, and a mass element. From the perspective of power flow, part of the energy flowing to the wheel will be absorbed by the DVA and transformed into the potential energy of the elastic element, the internal energy of the damping element, and the kinetic energy of the mass element. The three parameters of the DVA directly determine its vibration suppression effect. Therefore, including the suspension stiffness and damping, there are a total of five parameters to be determined.

To narrow down the range of parameter optimization to improve efficiency, the sensitivities of VBA, SRS, and DWL to system parameter changes were investigated. The initial mass of DVA is taken to be 0.1 times the unsprung mass, i.e., $m_3 = 0.1m_1 = 4.54$ kg. To attenuate the high-frequency vibration of the wheel, the inherent frequency of the DVA ($f_3 = 1/2\pi \times \sqrt{k_3/m_3}$) should theoretically be equal to the offset frequency of the wheel ($f_1 = 1/2\pi \times \sqrt{(k_1 + k_2)/m_1}$). Thus, the initial stiffness of DVA can be determined as $k_3 = 35290$ N/m. The damping ratio of the DVA ($\xi_3 = c_3/2\sqrt{m_3k_3}$) is generally taken as 0.1 to 0.3, and 0.2 is taken here, corresponding to an initial damping of $c_3 = 160$ Ns/m. Assuming that the vehicle is travelling at 60 km/h on a class C road and the variation range of the five parameters is 0.2 to 1.8 times the initial values, the RMS values of the three evaluation indicators were calculated. Figure 11 plots the normalized performance of the changes in suspension stiffness, suspension damping, DVA mass, DVA stiffness, and DVA damping, respectively.

As shown in Figures 11(a) and 11(b), the VBA increases with the increasing suspension stiffness, while the DWL does the opposite. As the suspension damping increases, the VBA first decreases and then increases, and the optimal suspension damping for ride comfort is shown at $0.4c_1$. Furthermore, it can be seen that the suspension damping has the greatest effect on the SRS, which should be constrained during the parameter optimization. As shown in Figures 11(c)–11(e), the trend of VBA with the change of DVA parameters is similar to that of DWL. However, the SRS is hardly affected by the change in the DVA parameters. Specifically, the VBA and DWL decrease with increasing DVA mass and first decrease and then increase with increasing DVA stiffness and damping. The optimal DVA stiffness for ride comfort is shown at $0.9k_3$ while it is $1.3k_3$ for the best handling performance concern. The optimal DVA damping for ride comfort and handling performance is shown at $0.7c_2$ and $0.5c_2$, respectively. The optimization range of DVA parameters can be finally reduced to m_3~$1.8m_3$, $0.5k_3$~$1.5k_3$, and $0.2c_2$~c_2.

4.2. Optimization of System Parameters. The above determination of system parameters is a typical multiobjective optimization problem with five optimization variables, and the optimization objectives include handling performance and ride comfort. To improve handling performance, the RMS value of DWL should be minimized, while to improve ride comfort, the RMS value of VBA should be minimized. The optimization objectives can be expressed as follows:

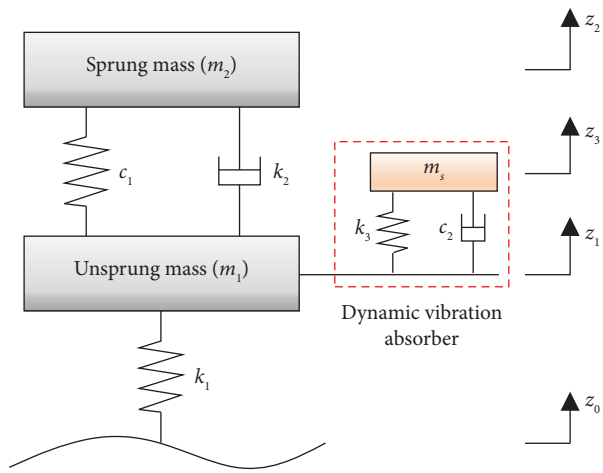

Figure 10: NVDS-based system model.

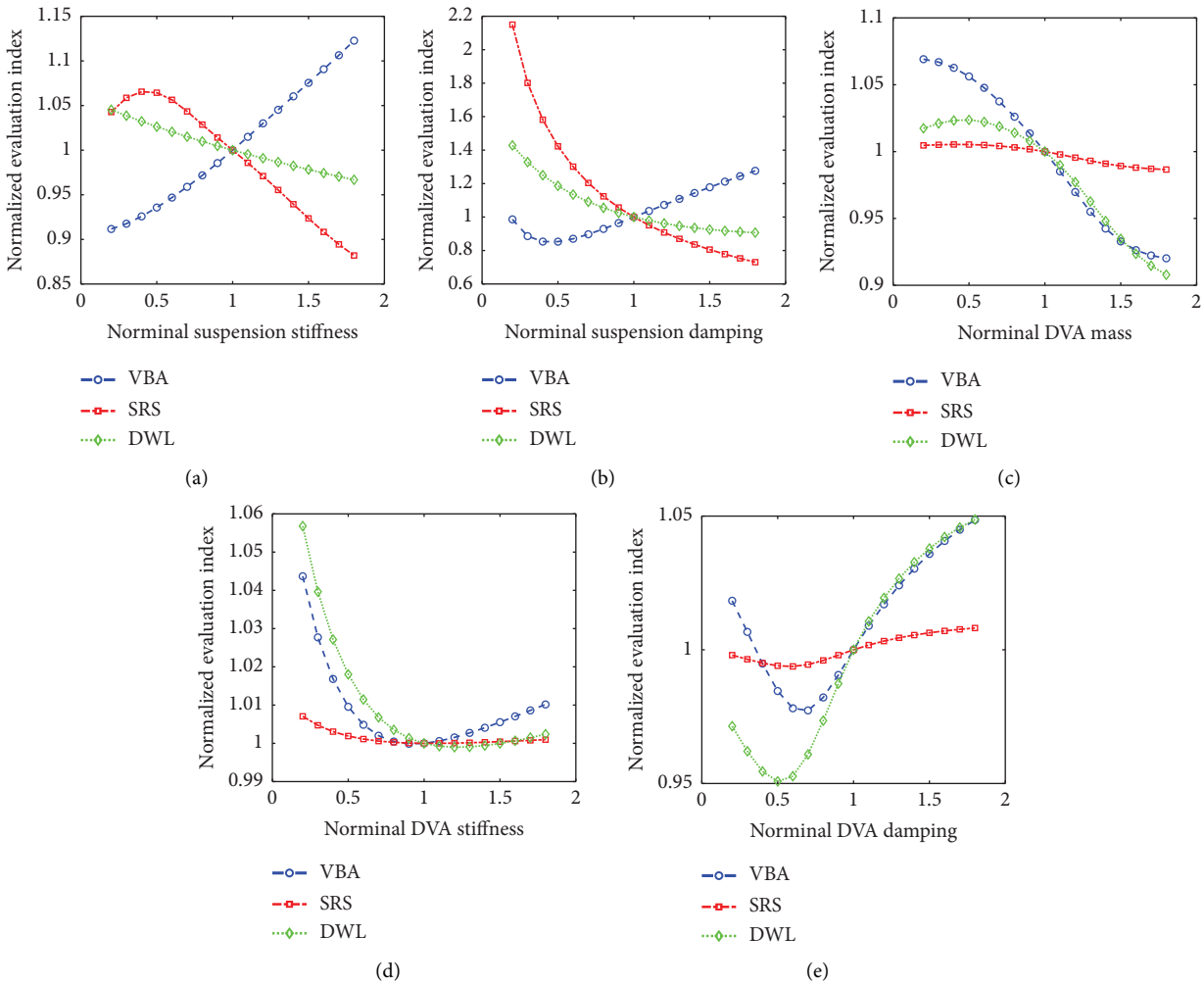

Figure 11: Effects of different parameters on vehicle performances: (a) suspension stiffness; (b) suspension damping; (c) DVA mass; (d) DVA stiffness; (e) DVA damping.

$$\begin{cases} f_1(\mathbf{x}) = \sigma_{F_d}, \\ f_2(\mathbf{x}) = \sigma_{\ddot{z}_2}, \end{cases} \tag{22}$$

where $\mathbf{x} = [\, k_2 \;\; c_1 \;\; m_3 \;\; k_3 \;\; c_2 \,]$ is the parameter vector to be optimized and σ_{F_d} and $\sigma_{\ddot{z}_2}$ are the RMS values of the DWL and VBA.

Then, the multiobjective optimization problem is formulated as follows:

$$\min F(\mathbf{x}) = \{f_1(\mathbf{x}), f_2(\mathbf{x})\}, \tag{23}$$

subject to the following constraints:

$$\begin{cases} g_1 = l - |z_2 - z_1| \geq 0, \\ g_2 = l - |z_3 - z_1| \geq 0, \\ 4000\,(\text{kg}) \leq k_2 \leq 36000\,(\text{kg}), \\ 300\,(\text{Ns}/m) \leq c_1 \leq 2700\,(\text{Ns}/m), \\ 4.54\,(\text{kg}) \leq m_3 \leq 8.172\,(\text{kg}), \\ 17645\,(N/m) \leq k_3 \leq 52935\,(N/m), \\ 32\,(\text{Ns}/m) \leq c_2 \leq 160\,(\text{Ns}/m), \end{cases} \tag{24}$$

where g_1 and g_2 are the constraints of working space for the suspension and DVA and $l = 0.06$ m denotes the maximum travel.

In this study, a GA is used to determine the optimal parameters, which have been proven to be suitable for solving the multiobjective optimization problems [36]. The relevant settings of the GA are as follows:

(1) The population size is set to 100, and the number of elites is set to 10;

(2) The competitive selection method is used, and the competitive scale is set to 10;

(3) The crossover method selects the arithmetic crossover method;

(4) The single point genetic mutation is adopted, and the mutation probability is set to 0.02 to coordinate the solution speed and the diversity of the population;

(5) The termination condition adopts the combination of termination algebra and evolution trends. The GA will be terminated when the change of the fitness function value is less than 0.1% for 10 consecutive generations or after 100 consecutive generations of evolution.

The quarter-vehicle model described by equation (21) was used as the iterative model, the class C road was selected as the model input, and the vehicle speed was set to 60 km/h. The execution of the GA yields the pareto-optimal front given in Figure 12. As shown in the figure, an improvement in handling performance will inevitably lead to a deterioration in ride comfort. Considering that the increase in wheel mass and stiffness mainly affects vehicle handling performance, followed by ride comfort, an optimal solution considering 80% handling performance and 20% ride comfort was chosen to enhance the comprehensive performance of the vehicle with NPWs. The optimized parameters are shown in Table 1.

5. Simulation Results and Discussion

To validate the correctness of the parameter optimization and the effectiveness of the proposed NVDS, the frequency-domain response analysis and dynamics simulation were performed. For the sake of the simplicity, the systems to be compared are named as follows:

(i) Passive system: quarter-vehicle system modelled by equation (2)

(ii) NVDS-based system: quarter-vehicle system with NVDS, as shown in equation (21).

5.1. Analysis of Frequency-Domain Response. For the NVDS-based system described in equation (21), the Laplace transform yields

$$\begin{cases} m_2 z_2 s^2 + c_1(z_2 s - z_1 s) + k_2(z_2 - z_1) = 0, \\ m_3 z_3 s^2 + c_2(z_3 s - z_1 s) + k_3(z_3 - z_1) = 0, \\ m_1 z_1 s^2 - c_2(z_3 s - z_1 s) - c_1(z_2 s - z_1 s) - k_3(z_3 - z_1) - k_2(z_2 - z_1) \\ + k_1(z_1 - z_0) = 0. \end{cases} \tag{25}$$

Then, the transfer function between z_2 and z_1, z_3 and z_1, and z_1 and z_0 can be obtained by equation (25) as follows:

$$\frac{z_2}{z_1} = \frac{A_1}{A_2}, \tag{26}$$

$$\frac{z_3}{z_1} = \frac{A_3}{A_4}, \tag{27}$$

$$\frac{z_1}{z_0} = \frac{k_1 A_2 A_4}{A_2 A_4 A_5 - A_1^2 A_4 - A_2 A_3^2}, \tag{28}$$

where $A_1 = c_1 s + k_2$, $A_2 = m_2 s^2 + c_1 s + k_2$, $A_3 = c_2 s + k_3$, $A_4 = m_3 s^2 + c_2 s + k_3$, and $A_5 = m_1 s^2 + c_2 s + c_1 s + k_3 + k_2 + k_1$.

The amplitude-frequency characteristic of the VBA $\ddot{z}_2$ to the road excitation speed $\dot{z}_0$ can be expressed as follows:

$$|H(j\omega)|_{\ddot{z}_2 \sim \dot{z}_0} = \left|\frac{\ddot{z}_2}{\dot{z}_0}\right| = \omega \left|\frac{z_2}{z_0}\right| = \omega \times \left|\frac{z_2}{z_1}\right| \times \left|\frac{z_1}{z_0}\right|. \tag{29}$$

Substituting equations (26) and (28) into equation (29) we get

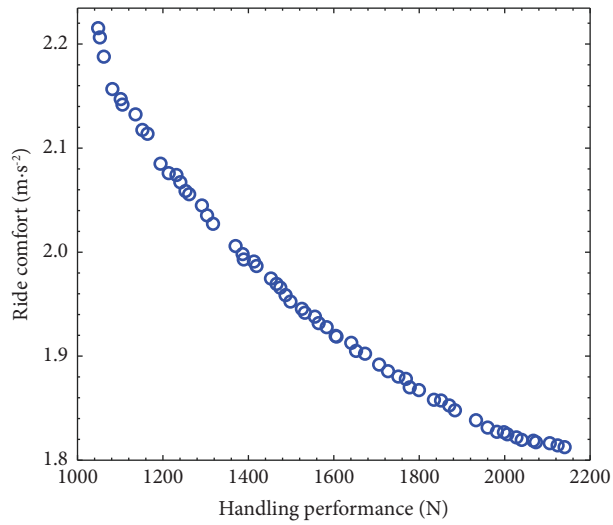

Figure 12: The pareto-optimal front between the handling performance and ride comfort.

Table 1: System parameters before and after optimization.

Parameter	Initial value	Optimized value
k_2 (N/m)	20000	16487.8
c_1 (Ns/m)	1500	1665.9
m_3 (kg)	4.54	8.16
k_3 (N/m)	35290	30896.3
c_2 (Ns/m)	160	125.8

$$|H(j\omega)|_{\ddot{z}_2 \sim \dot{z}_0} = \left| \frac{\omega A_1 A_4 k_1}{A_2 A_4 A_5 - A_1^2 A_4 - A_2 A_3^2} \right|. \quad (30)$$

The amplitude-frequency characteristic of the SRS f_d to the road excitation speed $\dot{z}_0$ can be expressed as follows:

$$|H(j\omega)|_{f_d \sim \dot{z}_0} = \left| \frac{f_d}{\dot{z}_0} \right| = \frac{1}{\omega} \left| \frac{z_2 - z_1}{z_0} \right|. \quad (31)$$

Substituting equations (26) and (28) into equation (31) we get

$$|H(j\omega)|_{f_d \sim \dot{z}_0} = \left| \frac{k_1 (A_1 A_4 - A_2 A_4)}{\omega \left(A_2 A_4 A_5 - A_1^2 A_4 - A_2 A_3^2 \right)} \right|. \quad (32)$$

The amplitude-frequency characteristic of the relative DWL F_d/G to the road excitation speed $\dot{z}_0$ can be expressed as follows:

$$|H(j\omega)|_{F_d/G \sim \dot{z}_0} = \left| \frac{F_d/G}{\dot{z}_0} \right| = \left| \frac{z_1 - z_0}{z_0} \right| \times \frac{k_1}{\omega (m_1 + m_2 + m_3) g}, \quad (33)$$

where $F_d = k_1 (z_1 - z_0)$ is the DWL and $G = (m_1 + m_2) g$ is the static wheel load.

Substituting equation (28) into equation (33) we get

$$|H(j\omega)|_{F_d/G \sim \dot{z}_0} = \left| \frac{k_1 \left[k_1 A_2 A_4 - \left(A_2 A_4 A_5 - A_1^2 A_4 - A_2 A_3^2 \right) \right]}{\omega \left(A_2 A_4 A_5 - A_1^2 A_4 - A_2 A_3^2 \right) (m_1 + m_2 + m_3) g} \right|. \quad (34)$$

According to above derivation, the amplitude-frequency characteristics of the two systems are compared in Figure 13.

Due to the introduction of DVA, the amplitude-frequency characteristic curves of VBA and DWL for the NVDS-based system show three resonance peaks, as shown in Figures 13(a) and 13(c). The amplitude-frequency characteristic curve of the SRS shown in Figure 13(b), on the other hand, only has one obvious resonance peak. Furthermore, it can be seen that the amplitude of the NVDS-based system is significantly less than that of the passive system in the case of body resonance and wheel resonance, although it is slightly larger within the 3~9 Hz frequency range. In general, the ride comfort and handling performance of the NVDS-based system are effectively improved. Within the 1~50 Hz, the amplitude-frequency characteristic curve of the SRS of the NVDS-based system is always below that of the passive system. Therefore, the proposed NVDS can reduce the probability of a strike between suspension springs and the limit block.

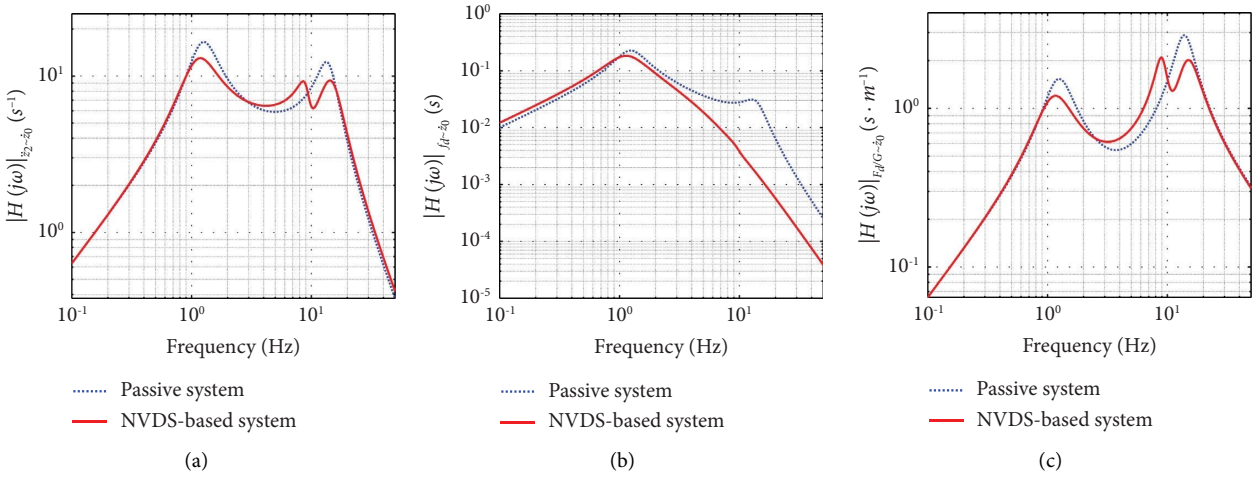

Figure 13: Amplitude-frequency characteristic curves after optimization: (a) $\ddot{z}_2 \sim \dot{z}_0$; (b) $f_d \sim \dot{z}_0$; (c) $F_d/G \sim \dot{z}_0$.

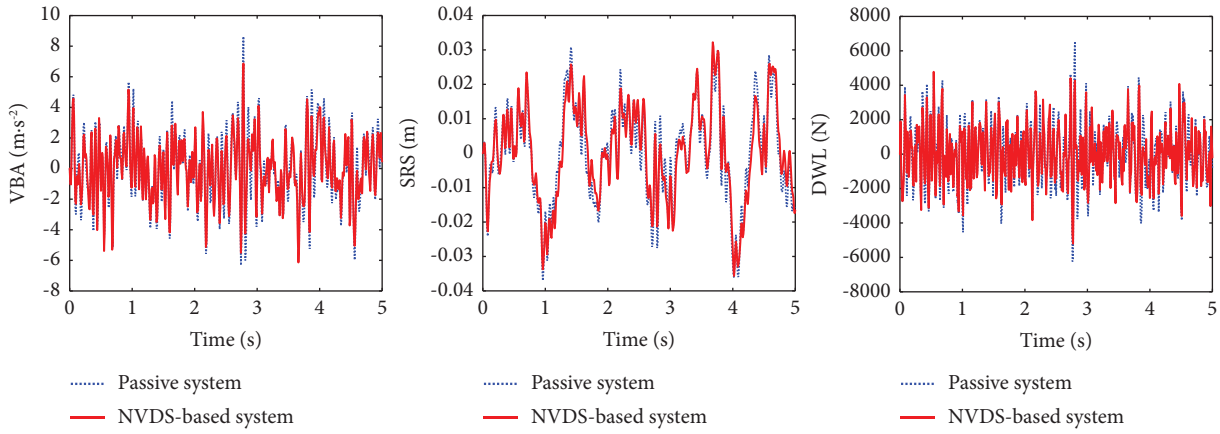

Figure 14: Comparison of dynamic performance on the random road.

Table 2: Simulation results under random road excitation.

Index (RMS value)	Passive system	NVDS-based system	Improvement (%)
VBA ($m \cdot s^{-2}$)	2.29	2.02	11.8
SRS (m)	0.0141	0.0138	2.1
DWL (N)	1816.06	1590.86	12.4

5.2. Dynamics Simulation under Random Road Excitation. Assuming that the vehicle runs on the class C road at the speed of 60 km/h, Figure 14 gives a comparison of VBA, SRS, and DWL for the two systems.

It can be observed from the figure that under the random road excitation, the NVDS-based system generates a good improvement on both the VBA and DWL compared to the passive system. The SRS of the two systems is always within the maximum travel. The specific comparison of the RMS values of the three evaluation indicators is shown in Table 2. It can be seen that the DWL and VBA of the NVDS-based system decreased by 12.4% and 11.8%, respectively, compared to the passive system. This suggests that the proposed NVDS can effectively enhance the handling performance and ride comfort of the vehicle with NPWs on the random road.

5.3. Dynamics Simulation under Bump Road Excitation. Using the bump road excitation described in equation (7) as the system input and the vehicle speed set to 36 km/h, a comparison of the dynamic response of different systems are obtained, as shown in Figure 15.

It can be seen from Figure 15 that the proposed NVDS-based system outperforms the passive system with a smaller VBA, SRS, and DWL amplitude. To better evaluate the performance differences between the two systems, a quantitative analysis was performed using the peak-to-peak values, representing the difference between the maximum and minimum values, as shown in Table 3. According to Table 3, the application of the NVDS can reduce 9.1% of the VBA, 3.5% of the SRS and 7.7% of the DWL. Besides the peak-to-peak value, the convergence time is also an important indicator to evaluate the

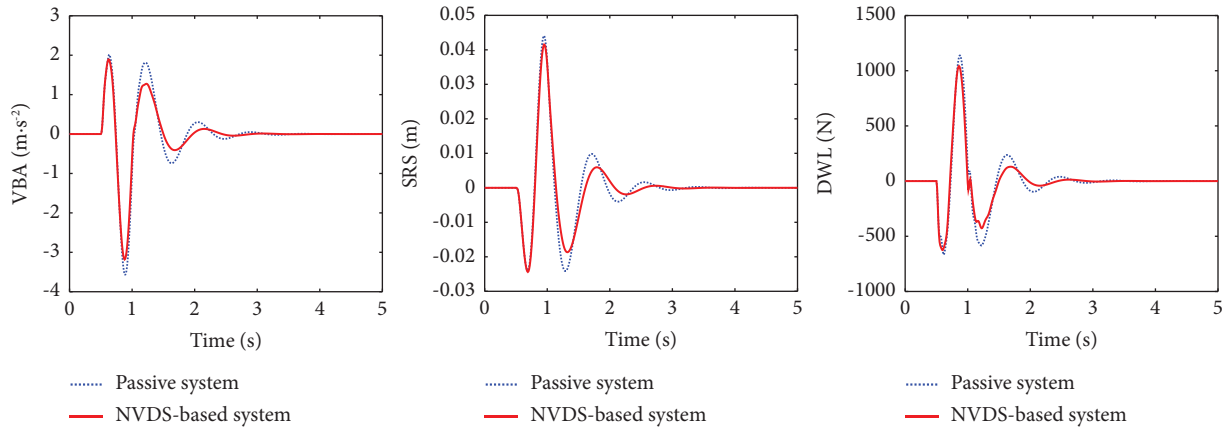

Figure 15: Comparison of dynamic performance on the bump road.

Table 3: Simulation results under bumpy road excitation.

Index (peak-to-peak value)	Passive system	NVDS-based system	Improvement (%)
VBA (m·s^{-2})	5.58	5.07	9.1
SRS (m)	0.0683	0.0659	3.5
DWL (N)	1805.78	1667.04	7.7

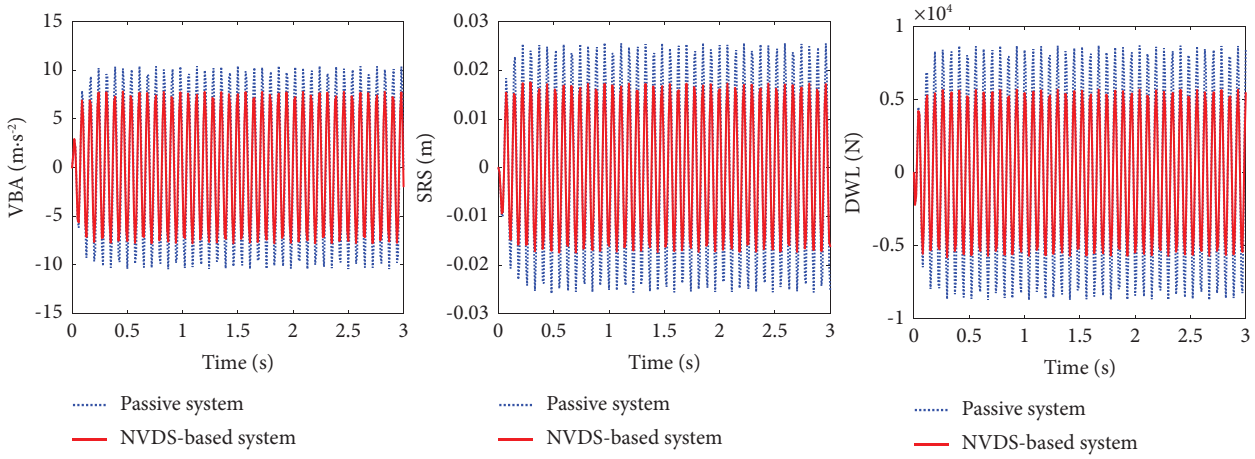

Figure 16: Comparison of dynamic performance on the sinusoidal road.

Table 4: Simulation results under sinusoidal road excitation.

Index (peak-to-peak value)	Passive system	NVDS-based system	Improvement (%)
VBA (m·s^{-2})	20.87	15.60	25.3
SRS (m)	0.0515	0.0349	32.2
DWL (N)	1740.45	1147.54	34.1

dynamic performance of the system under the bump road excitation. As shown in Figure 15, it is clear that the convergence time of the dynamic response of the NVDS-based system is shorter than that of the passive system. In other words, the NVDS-based system can recover the steady-state response at a faster rate after driving over a bump. The comparison of peak-to-peak values and convergence times indicates that the NVDS-based system provides better handling performance on bumpy roads as well as ride comfort compared to the passive system.

5.4. Dynamics Simulation under Sinusoidal Road Excitation. A sinusoidal signal with an amplitude of 0.01 m and a frequency of 13.5 Hz was selected as the input to analyse the dynamic response of the system in the case of wheel resonance. The dynamic response of the two systems is shown in Figure 16.

It can be seen that the proposed NVDS-based system outperforms the passive system in terms of both VBA and DWL under sinusoidal road excitation with wheel resonance frequency. The peak-to-peak values representing the difference

between the maximum and minimum values were used to quantitatively evaluate the dynamic response of the vehicle, as shown in Table 4. It is clear that compared to the passive system, the NVDS-based system yields 25.3%, 32.2%, and 34.1% reductions in the VBA, SRS, and DWL, respectively. In other words, the application of NVDS significantly enhances the ride comfort and handling performance of the vehicle in cases of the wheel resonance, reducing the damage to the vehicle and passengers induced by wheel resonance.

6. Conclusion

In this article, a DVA-based NVDS is proposed for the vehicle with NPWs to improve the dynamic performance. First, the effective vertical stiffness of the selected NPW was identified through a static load-deflection experiment. Next, the effects of NPW mass and vertical stiffness on vehicle dynamic performance were investigated in terms of frequency domain response, time domain response, and power flow. Then, a DVA-based NVDS was designed, and its optimal parameters are determined by multiobjective GA. In the end, the handling performance and ride comfort of the vehicle with NPWs are improved. The major conclusions can be drawn as follows:

(1) Compared with the reference pneumatic wheel, the NPW selected in this case presents greater mass and higher vertical stiffness, which will aggravate the high-frequency vibration of the vehicle and cause an increase in wheel resonance frequency.

(2) Compared to vehicle speed, road roughness has a greater impact on vehicle dynamic performance, and its increase leads to a significant deterioration of vehicle dynamic performance, especially handling performance.

(3) The proposed NVDS can effectively reduce the vibration response in the case of vehicle body and wheel resonance, enhancing the ride comfort and handling performance of vehicles with higher wheel mass and stiffness. Specifically, the RMS/peak-to-peak values of the DWL and VBA for the NVDS-based system are improved by 12.4% and 11.8% on the random road and by 34.1% and 25.3% on the sinusoidal road, respectively.

This study could provide a reference for the design of vehicle chassis and the performance matching of NPWs (with higher mass and stiffness) with vehicle vibration damping systems. In future work, the DVA prototype will be fabricated for experiments to explore the effects of NVDS in practical applications.

Data Availability

The data used to support the findings of this study are available from the corresponding author upon request.

Conflicts of Interest

The authors declare that there are no conflicts of interest regarding the publication of this article.

Acknowledgments

The work described in this paper was fully supported by a grant from Open fund of State Key Laboratory of Automotive Simulation and Control (Project 20210204).

References

[1] Y. Zhao, X. Du, F. Lin, Q. Wang, and H. Fu, "Static stiffness characteristics of a new non-pneumatic tire with different hinge structure and distribution," *Journal of Mechanical Science and Technology*, vol. 32, no. 7, pp. 3057–3064, 2018.

[2] Z. Zheng, S. Rakheja, and R. Sedaghati, "A comparative study of static and dynamic properties of honeycomb non-pneumatic wheels and a pneumatic wheel," *Proceedings of the Institution of Mechanical Engineers-Part D: Journal of Automobile Engineering*, vol. 235, no. 14, pp. 3631–3646, 2021.

[3] J. Sim, J. Hong, I. Cho, and J. Lee, "Analysis of vertical stiffness characteristics based on spoke shape of non-pneumatic tire," *Applied Sciences*, vol. 11, no. 5, 2021.

[4] J. R. Cho, J. H. Lee, K. M. Jeong, and K. W. Kim, "Optimum design of run-flat tire insert rubber by genetic algorithm," *Finite Elements in Analysis and Design*, vol. 52, pp. 60–70, 2012.

[5] W. Li, X. Liu, A. Sun et al., "Exploring piperazine for intrinsic weather-proof, robust and self-healable poly (urethane urea) toward surface and tire protection," *Polymer*, vol. 227, Article ID 123829, 2021.

[6] L. Zang, X. Wang, C. Wu, F. Teng, and S. Yang, "Analysis of load characteristic and contact patch characteristic of support insert run-flat tire under zero-pressure condition," *International Journal of Automotive Technology*, vol. 22, no. 5, pp. 1141–1151, 2021.

[7] K. W. Kim and C. W. Kwark, "Introduction to technology trends, problems and solutions of non-pneumatic," *Transactions of the Korean Society of Automotive Engineers*, vol. 41, pp. 26–31, 2019.

[8] J. Ma, J. D. Summers, P. Joseph, and A. Kolla, *Dynamic Simulation of Interaction between Non-pneumatic Tire and Sand*, SAE Technical Paper, Warrendale, PA, USA, 2010.

[9] X. Jin, C. Hou, X. Fan, Y. Sun, J. Lv, and C. Lu, "Investigation on the static and dynamic behaviors of non-pneumatic tires with honeycomb spokes," *Composite Structures*, vol. 187, pp. 27–35, 2018.

[10] L. Wei, X. Zhao, Q. Yu, and G. Zhu, "A novel star auxetic honeycomb with enhanced in-plane crushing strength," *Thin-Walled Structures*, vol. 149, Article ID 106623, 2020.

[11] L. Zang, X. Wang, P. Yan, and Z. Zhao, "Structural design and characteristics of a non-pneumatic tire with honeycomb structure," *Mechanics of Advanced Materials and Structures*, vol. 29, no. 25, pp. 4066–4073, 2022.

[12] J. Ju, D. M. Kim, and K. Kim, "Flexible cellular solid spokes of a non-pneumatic tire," *Composite Structures*, vol. 94, no. 8, pp. 2285–2295, 2012.

[13] R. Rugsaj and C. Suvanjumrat, "Proper radial spokes of non-pneumatic tire for vertical load supporting by finite element analysis," *International Journal of Automotive Technology*, vol. 20, no. 4, pp. 801–812, 2019.

[14] H. Li, Y. Zhao, F. Lin, and M. Zhu, "Nonlinear dynamics modeling and rollover control of an off-road vehicle with mechanical elastic wheel," *Journal of the Brazilian Society of Mechanical Sciences and Engineering*, vol. 40, no. 2, 2018.

[15] X. Du, Y. Zhao, F. Lin, H. Fu, and Q. Wang, "Numerical and experimental investigation on the camber performance of

a non-pneumatic mechanical elastic wheel," *Journal of the Brazilian Society of Mechanical Sciences and Engineering*, vol. 39, no. 9, pp. 3315–3327, 2017.

[16] Y. Deng, Y. Zhao, F. Lin, Z. Xiao, M. Zhu, and H. Li, "Simulation of steady-state rolling non-pneumatic mechanical elastic wheel using finite element method," *Simulation Modelling Practice and Theory*, vol. 85, pp. 60–79, 2018.

[17] Z. Zhang, H. Fu, Q. Zhao, D. Tan, and K. Yang, "Pattern design and performance analysis of a flexible spoke bionic non-pneumatic tire," *Journal of the Brazilian Society of Mechanical Sciences and Engineering*, vol. 43, no. 1, 2021.

[18] A. Gasmi, P. F. Joseph, T. B. Rhyne, and S. M. Cron, "Development of a two-dimensional model of a compliant non-pneumatic tire," *International Journal of Solids and Structures*, vol. 49, no. 13, pp. 1723–1740, 2012.

[19] C. Liang, W. Wei, H. Mousavi, K. Chen, B. Asafo-Duho, and G. Wang, "Investigation on static grounding analysis model of non-pneumatic tire with nonlinear spokes," *AIP Advances*, vol. 11, no. 1, Article ID 015303, 2021.

[20] J. Ma, J. D. Summers, and P. F. Joseph, "Numerical investigation of effect of membrane thickness on the performance of cellular shear band based non-pneumatic tire," in *Proceedings of the International Design Engineering Technical Conferences and Computers and Information in Engineering Conference*, vol. 8, pp. 781–791, Washington, DC, USA, August 2012.

[21] S. Ludvigsen, Z. Andleeb, H. A. Khawaja, M. Moatamedi, and B. Alzahabi, "Multiphysics analysis of contact pressure profile of airless tires as compared to conventional tires," *Multiphysics Simulations in Automotive and Aerospace Applications*, vol. 14, pp. 21–49, 2021.

[22] J. Ju, M. Veeramurthy, J. D. Summers, and L. Thompson, "Rolling resistance of a nonpneumatic tire having a porous elastomer composite shear band," *Tire Science and Technology*, vol. 41, no. 3, pp. 154–173, 2013.

[23] V. V. Mazur, "Experiments to find the rolling resistance of non-pneumatic tires car wheels," in *Proceedings of the 5th International Conference on Industrial Engineering (ICIE 2019)*, vol. 15, pp. 641–648, Berlin, Germany, December 2020.

[24] H. Fu, X. Chen, Q. Zhao, Z. Xiao, and X. Liang, "Fatigue life prediction and influencing factors analysis of mesh flexible spoke non-pneumatic tire," *Advances in Mechanical Engineering*, vol. 13, no. 10, Article ID 168781402110524, 2021.

[25] H. Fu, X. Liang, Y. Wang, L. Ku, and Z. Xiao, "Thermal mechanical coupling analysis of a flexible spoke non-pneumatic tire," *Strojniški vestnik-Journal of Mechanical Engineering*, vol. 68, no. 3, pp. 143–154, 2022.

[26] Y. Zhao, H. Xu, Y. Deng, and Q. Wang, "Multi-objective optimization for ride comfort of hydro-pneumatic suspension vehicles with mechanical elastic wheel," *Proceedings of the Institution of Mechanical Engineers-Part D: Journal of Automobile Engineering*, vol. 233, no. 11, pp. 2714–2728, 2019.

[27] R. Rugsaj and C. Suvanjumrat, "Study of geometric effects on nonpneumatic tire spoke structures using finite element method," *Mechanics Based Design of Structures and Machines*, vol. 50, no. 7, pp. 2379–2399, 2022.

[28] P. Dhrangdhariya, S. Maiti, and B. Rai, "Effect of spoke design and material nonlinearity on non-pneumatic tire stiffness and durability performance," 2021, https://arxiv.org/abs/2103.03637.

[29] H. Zhou, H. Li, Y. Mei, G. Wang, C. Liu, and L. Zhang, "Research on vibration reduction method of nonpneumatic tire spoke based on the mechanical properties of domestic cat's paw pads," *Applied Bionics and Biomechanics*, vol. 2021, Article ID 9976488, 16 pages, 2021.

[30] Q. Wang, Y. Zhao, H. Xu, and Y. Deng, "Adaptive backstepping control with grey signal predictor for nonlinear active suspension system matching mechanical elastic wheel," *Mechanical Systems and Signal Processing*, vol. 131, pp. 97–111, 2019.

[31] W. Liu, R. Wang, R. Ding, X. Meng, and L. Yang, "On-line estimation of road profile in semi-active suspension based on unsprung mass acceleration," *Mechanical Systems and Signal Processing*, vol. 135, Article ID 106370, 2020.

[32] P. Múčka, "Simulated road profiles according to ISO 8608 in vibration analysis," *Journal of Testing and Evaluation*, vol. 46, no. 1, pp. 405–418, 2017.

[33] H. Jiang, C. Wang, Z. Li, and C. Liu, "Hybrid model predictive control of semi-active suspension in electric vehicle with hub-motor," *Applied Sciences*, vol. 11, no. 1, p. 382, 2021.

[34] P. Shi, P. Shi, C. Yan, R. Zhang, and P. Xiao, "Analysis of the electric wheel vibration reduction system of a wheel-hub motor-driven vehicle," *Proceedings of the Institution of Mechanical Engineers-Part C: Journal of Mechanical Engineering Science*, vol. 233, no. 3, pp. 848–856, 2019.

[35] T. P. J. van der Sande, M. H. M. Merks, E. Lindeman, and H. Nijmeijer, "Rule-based control of a semi-active suspension system for road holding using limited sensor information: design and experiments," *Vehicle System Dynamics*, vol. 60, no. 12, pp. 4226–4244, 2022.

[36] H. Tamaki, H. Kita, and S. Kobayashi, "Multi-objective optimization by genetic algorithms: a review," in *Proceedings of the IEEE international conference on evolutionary computation*, pp. 517–522, Nagoya, Japan, May 1996.